

Model development and numerical simulation of electric-stimulus-responsive hydrogels subject to an externally applied electric field

Hua Li^{a,*}, Z. Yuan^a, K.Y. Lam^a, H.P. Lee^a, Jun Chen^a, Justin Hanes^b, Jie Fu^b

^a Institute of High Performance Computing, National University of Singapore, 1 Science Park Road, #01-01 The Capricorn, Singapore Science Park II, Singapore 117528, Singapore

^b Department of Chemical Engineering, The Johns Hopkins University, 3400 N. Charles Street, 221 MD Hall, Baltimore, MD 21218, USA

Received 10 June 2003; received in revised form 13 October 2003; accepted 14 October 2003

Abstract

Based on a multi-phasic mixture theory with consideration of ionic diffusion and convection, a multi-physic model, called the multi-effect-coupling electric-stimulus (MECe) model, is developed for simulation of responsive behavior of the electric-sensitive hydrogels when they are immersed into a bathing solution subject to an externally applied electric field. In the developed model, with chemo-electro-mechanical coupling effects, the convection–diffusion equations for concentration distribution of diffusive ions incorporate the influence of electric potential. The electroneutrality condition is replaced by the Poisson equation for distribution of electric potential. The steady and transient analyses of hydrogel deformation are easily carried out by the continuity and momentum equations of the mixture phase. Further, the computational domain of the present model covers both the hydrogel and the surrounding solution. In order to solve the present mathematical model consisting of multi-field coupled nonlinear partial differential governing equations, a hierarchical iteration technique is proposed and a meshless Hermite–Cloud method (HCM) is employed. The steady-state simulation of the electric-stimulus responsive hydrogel is numerically conducted when it is subjected to an externally applied electric field. The hydrogel deformation and the ionic concentrations as well as electric potentials of both the hydrogel and external solution are investigated. The parameter influences on the swelling behaviors of the hydrogel are also discussed in detail. The simulating results are in good agreement with the experimental data and they validate the presently developed model.

© 2003 Elsevier B.V. All rights reserved.

Keywords: Electric-stimulus responsive hydrogels; Multiphasic mixture theory; Mathematical model; Diffusion; Convection; BioMEMS; Meshless method

1. Introduction

Recently biosensors/actuators, made of stimuli-responsive polymeric hydrogels, have attracted much attention for their wide-range biological applications in drug delivery, artificial muscle and BioMEMS, such as hydrogel-actuated microvalves and microfluidic controllers in microchannels (Brock et al., 1994; Shahinpoor, 1995; Beebe et al., 2000; Kim and Peppas, 2002; Baldi et al., 2002). Their capability of reversible volume change makes them have potential BioMEMS application, where large swelling and shrinking of the hydrogels are desired when they are induced by bio-stimuli, e.g. pH, temperature and electric field (de Gennes et al., 2000; Eichenbaum et al., 1998; Miyata et al., 1999;

Nemat-Nasser and Li, 2000). In particular, electric-sensitive hydrogels with biocompatibility and biostability are more attractive as they are able to implement an isothermal energy conversion from chemical free energy directly to mechanical work, actuated by an external electric stimulus. As such, the mechanical energy is triggered by an electric signal. This results in one of their important functions as biosensors/actuators, in which the electric-stimulus responsive hydrogels with fixed-charge groups can bend reversibly when they are subjected to an externally applied electric field. Usually the electric-sensitive hydrogels are composed of electrolytes and a swellable and insoluble crosslinked polymer network with fixed-charge groups, as shown in Fig. 1. When the hydrogels are immersed into a bathing solution under an externally applied electric field, the hydrogels deform. They swell and bend due to the pressure difference of both hydrostatic and osmotic pressures, which

* Corresponding author. Tel.: +65-641-91561; fax: +65-641-91380.
E-mail address: lihua@ihpc.a-star.edu.sg (H. Li).

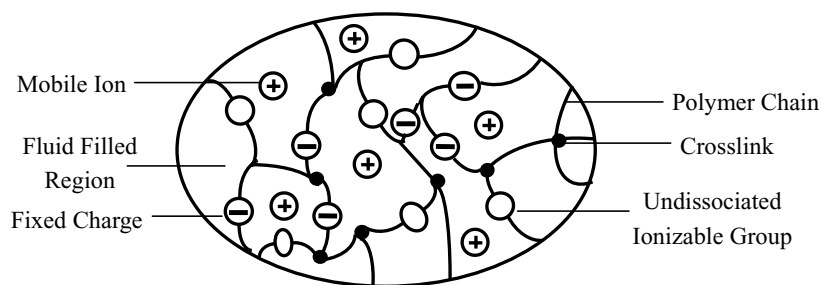


Fig. 1. Micro view of the hydrogel structure.

are caused by ionic concentration difference between the internal hydrogels and the external solutions.

Many experiments have been performed to study the behavior of the hydrogels under the external electric field (Kim and Shin, 1999; Homma et al., 2000, 2001; Sun and Mak, 2001; Fei et al., 2002). However, the multiphysics characteristics of the hydrogels are not fully understood. Further, in the development of mathematical models of electric-stimuli responsive hydrogels, few studies have been made in the past decades. For example Grimshaw et al. (1990) and Shahinpoor (1994) developed the continuum models coupling multiphysics domains for the hydrogels. Shiga et al. (1993) studied a bending hydrogel due to the change of osmotic pressure. Doi et al. (1992) and Shahinpoor (2000) carried out the deformation analysis of the hydrogel subject to an external electric field. Brock et al. (1994) and Wang et al. (1997) investigated the dynamics of large-deformation hydrogels. However, it is difficult for these models to provide accurate simulations of the electric-stimulus responsive hydrogels, when they are immersed into the solution under an external electric field. Recently, Wallmersperger and Kroeplin (2001) and Zhou et al. (2002) made further studies of electric-sensitive hydrogels. However, the model developed by Wallmersperger and Kroeplin (2001) does not incorporate the mixture-phase continuity and can not directly compute the transient displacements. In the model developed by Zhou et al. (2002) for the steady-state analysis of equilibrium swelling hydrogel, no diffusive effect is considered, the electro-neutrality constraint has to be implemented and the computational domain excludes the surrounding solution. In addition, it is noted that the studies on hydrogel-like biological tissues are helpful for the investigation of electric-stimuli responsive hydrogels. They include the triphasic and multi-phasic mixture theories developed for the analysis of swelling and deformation of articular cartilage and other biological tissues (Lai et al., 1991, 2000; Mow et al., 1998; Hon et al., 1999; Gu et al., 1998, 1999).

In this paper, a novel mathematical model, called the multi-effect-coupling electric-stimulus (MECe) model, is developed with consideration of chemo-electro-mechanical coupling effects. In the MECe model, the continuity equations of the triphasic mixture theory for ion phases are modified to incorporate the electric-potential influence and convection–diffusion characteristics. The com-

putation of solid-phase displacement is explicit, and the simulated domain covers both the hydrogels and the surrounding solution. The governing equations of the presently developed model include (a) the continuity equations describing the solid and fluid phases, (b) the convection–diffusion equations computing the diffusive ion concentrations, (c) the Poisson equation for the electric field, and (d) the momentum equation for the mechanical response.

A novel meshless Hermite–Cloud method (HCM) based on a fixed kernel approximation (Li et al., 2003) is used to solve the challenging mathematical model here consisting of nonlinear coupling partial differential equations with remeshing requirement in hierarchical iteration procedure. The interpolation functions are constructed according to a set of points scattered in the problem domain and no background mesh is required. The point collocation technique is employed in the problem domain for discretization of the governing equations and boundary conditions. By the true meshless HCM, the nonlinear coupling partial differential governing equations are solved for simulation of the response characteristics of the electric-sensitive hydrogels subject to an externally applied electric field. The numerically computed results are obtained for the distributions of diffusive ionic concentrations and electric potentials in both the interior of hydrogels and the exterior solution, and the swelling and bending deformations of the hydrogels. Compared with experimental data, a very good agreement is achieved. Moreover, several studies of the influence of the parameters on the hydrogel deformations are conducted to enhance the understanding of the chemo-electro-mechanical behaviors of the smart electric-stimuli responsive hydrogels.

2. Development of the MECe models

The classical triphasic and multi-phasic mixture models were developed for simulation of charged hydrated biological soft tissues (Lai et al., 1991, 2000; Mow et al., 1998; Hon et al., 1999; Gu et al., 1998, 1999). Zhou et al. (2002) extended the work to a steady-state analysis of hydrogel membrane under an external electric field. Based on their work, this paper develops the MECe model with the assumption that the ions flow, osmosize and redistribute in porous media

subject to an externally applied electric field. This results in the deformation of swelling, shrinking and bending of the porous media, such as the biological tissues and hydrogels (Yuan et al., 2002). The governing equations of the triphasic and multi-phase mixture models consist of the following equations.

The saturation condition is given by:

$$\phi^s + \phi^w + \sum_{k=1}^N \phi^k = 1 \quad (1)$$

in which ϕ^α ($\alpha = s, w, k$) are the volume fractions of solid network, water, and ionic species, respectively, N total number of electrolyte ionic species, $\phi^w = 1 - \phi_0^s / (1 + \text{Tr}(\mathbf{E}))$ (ϕ_0^s is the solid-phase volume fraction at a reference configuration and \mathbf{E} is the elastic strain vector of the solid-phase).

The continuity equations of water, solid network and ion phases are

$$\frac{\partial \rho^\alpha}{\partial t} + \nabla \cdot (\rho^\alpha \mathbf{v}^\alpha) = 0 \quad (\alpha = s, w, k) \quad (2)$$

where t is time, the apparent mass densities $\rho^\alpha = \rho_T^\alpha \phi^\alpha$ ($\alpha = w, s$), $\rho^k = \rho_T^k \phi^k = c^k M_k \phi^w$ (c^k and M_k are the concentration and molar weight of the k th ionic species, respectively), ρ_T^α and \mathbf{v}^α ($\alpha = s, w, k$) are the true mass density and velocity vector of phase α .

The conservation of the fixed charge groups attached on the polymer network is given by:

$$\frac{\partial c^f}{\partial t} + \nabla \cdot (c^f \mathbf{v}^s) = 0, \quad \text{and} \quad c^f = \frac{c_0^f}{(1 + \text{Tr}(\mathbf{E})/\phi_0^w)} \quad (3)$$

in which, c_0^f and ϕ_0^w are the fixed charge density and the water volume fraction at the reference configuration, respectively.

The continuity equation of the mixture phase is given below by neglecting ϕ^k ($k = 1, 2, 3, \dots, N$) when they are compared with ϕ^s and ϕ^w

$$\nabla \cdot (\phi^s \mathbf{v}^s + \phi^w \mathbf{v}^w) = 0 \quad (4)$$

The momentum equations on neglecting the effects of body and inertial forces are given by

$$\text{mixture phase} \quad \nabla \cdot \boldsymbol{\sigma} = 0 \quad (5)$$

$$\begin{aligned} \text{water phase} \quad & -\rho^w \nabla \mu^w + f_{ws}(\mathbf{v}^s - \mathbf{v}^w) \\ & + \sum_{k=1}^N f_{wk}(\mathbf{v}^k - \mathbf{v}^w) = 0 \end{aligned} \quad (6)$$

$$\begin{aligned} \text{the } k\text{th ion phase} \quad & -\rho^k \nabla \mu^k + f_{ks}(\mathbf{v}^s - \mathbf{v}^k) \\ & + f_{kw}(\mathbf{v}^w - \mathbf{v}^k) + \sum_{j=1(j \neq k)}^N f_{kj}(\mathbf{v}^j - \mathbf{v}^k) \\ & = 0 \quad (k = 1, 2, 3, \dots, N) \end{aligned} \quad (7)$$

in which $\boldsymbol{\sigma}$ is the mixture stress, μ^α ($\alpha = w, k$) the chemical potential of phase α , $f_{\alpha\beta} = f_{\beta\alpha}$ are the frictional coefficients

corresponding to the resisting forces per mixture volume between phases α and β .

The electro-neutrality condition is

$$z^f c^f + \sum_{k=1}^N z^k c^k = 0 \quad (8)$$

in which z^k ($k = 1, 2, 3, \dots, N$) is the valence of ion k and the constitutive equations are

$$\boldsymbol{\sigma} = -p\mathbf{I} - T_c \mathbf{I} + \lambda_s \text{Tr}(\mathbf{E})\mathbf{I} + 2\mu_s \mathbf{E} \quad (9)$$

$$\mu^w = \mu_0^w + \frac{[p - RT \sum_{k=1}^N \Phi^k c^k + B_w \text{Tr}(\mathbf{E})]}{\rho_T^w} \quad (10)$$

$$\mu^k = \mu_0^k + \left(\frac{RT}{M_k} \right) \ln(\gamma_k c^k) + \frac{z^k F_c \psi}{M_k} \quad (11)$$

Additionally, the fluxes of water and ion are given as

$$J^w = \phi^w(\mathbf{v}^w - \mathbf{v}^s) \quad \text{and} \quad J^k = \phi^w c^k(\mathbf{v}^k - \mathbf{v}^s) \quad (12)$$

where p is the fluid pressure, \mathbf{I} the identity tensor, T_c the chemical expansion stress, Φ^k the osmotic coefficient of the k th ionic species. λ_s and μ_s are the Lamé coefficients of the solid matrix. γ_k is the activity coefficient of the k th ionic species, μ_0^α ($\alpha = w, k$) the chemical potential of phase α at the reference configuration. R and T are the universal gas constant and absolute temperature. F_c is the Faraday constant, ψ the electrical potential and B_w is the coupling coefficient.

The classical triphasic and multi-phasic mixture models, consisting of Eqs. (1)–(12), are unable to directly simulate the distribution of electrical potentials due to the use of electro-neutrality condition. The computational domain covers the porous media only. In order to overcome these drawbacks and take into account the chemo-electro-mechanical-coupling effects on both the domains of the hydrogels and the surrounding solution, the multiphysical MECe model is developed here for simulation of the multi-effect-coupling electric-stimulus responsive hydrogels based on the classical triphasic and multi-phasic mixture theories. The governing equations of the MECe model are derived as follows.

By summarizing Eqs. (6) and (7) for all of the N ionic species, and neglecting f_{ks} and f_{kj} when they are compared with f_{kw} (Lai et al., 2000), we have

$$f_{ws}(\mathbf{v}^s - \mathbf{v}^w) = \rho^w \nabla \mu^w + \sum_{k=1}^N \rho^k \nabla \mu^k \quad (13)$$

After substituting the constitutive Eqs. (10) and (11) into the above Eq. (13), taking $\rho^w = \rho_T^w \phi^w$ and $\rho^k = \rho_T^k \phi^k = c^k M_k \phi^w$, and on assuming the osmotic coefficients Φ^k ($k = 1, 2, \dots, N$) of all ionic species equal to Φ for an ideal solution without chemical reactions (Hon et al., 1999; Lai et al., 2000; Zhou et al., 2002), i.e. $\Phi^1 = \Phi^2 = \dots = \Phi^k = \dots =$

$\Phi^N = \Phi$ Eq. (13) can be rewritten

$$(\mathbf{v}^s - \mathbf{v}^w) = \left(\frac{\phi^w}{f_{ws}} \right) \left[\nabla p - RT(\Phi - 1) \nabla \left(\sum_{k=1}^N c^k \right) + B_w \nabla \text{Tr}(\mathbf{E}) + F_c \sum_{k=1}^N z^k c^k \nabla \psi \right] \quad (14)$$

where B_w is set to zero in the present computational simulations since its value is very small when $B_w \text{Tr}(\mathbf{E})$ is compared with the fluid pressure p (Lai et al., 1991; Sun et al., 1999; Hon et al., 1999; Zhou et al., 2002).

Compared with ϕ^s and ϕ^w , ϕ^k ($k = 1, 2, 3, \dots, N$) are very small and thus, they can be neglected. As a result, we have $\phi^s + \phi^w \approx 1$ by the saturation condition (1). Then, the continuity Eq. (4) is expressed as

$$\nabla \cdot \mathbf{v}^s + \nabla \cdot \phi^w (\mathbf{v}^w - \mathbf{v}^s) = 0 \quad (15)$$

On substituting Eq. (14) into Eq. (15) the continuity equation of the mixture phase is obtained

$$\nabla \cdot \mathbf{u}_t^s = \nabla \cdot \left\{ \left(\frac{(\phi^w)^2}{f_{ws}} \right) \left[\nabla p - RT(\Phi - 1) \nabla \left(\sum_{k=1}^N c^k \right) + F_c \sum_{k=1}^N z^k c^k \nabla \psi \right] \right\} \quad (16)$$

where \mathbf{u}^s is the displacement of the solid-phase and $\mathbf{u}_t^s = \mathbf{v}^s$.

In order to incorporate the effects of electrical potential in the modeling and simulation, unlike the classical triphasic and multi-phasic mixture models using the electro-neutrality constraint, the Nernst–Planck type of mass conservation equations for the divergence of each diffusive ionic flux is introduced as:

$$c_t^k = \nabla \cdot (D_k \nabla c^k) + \left(\frac{F_c}{RT} \right) z^k \nabla \cdot (c^k D_k \nabla \psi) - \nabla \cdot (c^k \mathbf{V}) + r_k(c^k) \quad (k = 1, 2, \dots, N) \quad (17)$$

This replaces Eq. (2) of the ionic phase. The following Poisson equation is employed to replace the electro-neutrality condition (8)

$$\nabla^2 \psi = - \frac{F_c}{\varepsilon \varepsilon_0} \sum_{k=1}^N (z^k c^k + z^f c^f) \quad (18)$$

where $\mathbf{V} = (\mathbf{v}^w - \mathbf{v}^s)$ is the fluid velocity relative to the polymer network and can be computed directly by Eq. (14). D_α is the diffusive coefficient, r_α the source term resulting from the chemical conversation of the molecules, ε the dielectric constants and ε_0 the permittivity of the free space.

So far, the development of the multiphysical MECe model has been completed for $(3 + N)$ unknown variables, p , \mathbf{u}^s , ψ and c^k ($k = 1, 2, \dots, N$). As a chemo-electro-mechanical coupled formulation with nonlinear partial differential equations, it consists of the momentum Eq. (5), the continuity

Eqs. (16) and (17) with the Eq. (14) and the Poisson Eq. (18). The developed MECe model is able to make the transient analysis for the kinetic behavior of the electric-sensitive hydrogels immersed in the bathing solution subject to an applied electric field, and to compute the distributions of ionic concentrations and electric potential in both the hydrogels and exterior solution. The MECe model can also be used for the steady-state simulation of equilibrium characteristics of the hydrogels. By neglecting the effects of convection and chemical conversion in the MECe governing Eqs. (5) and (16)–(18), a set of reduced governing equations is obtained for steady-state equilibrium analysis as expressed below.

The momentum equation by neglecting chemical expansion stress T_c is simplified to

$$\nabla \cdot \boldsymbol{\sigma} = \nabla \cdot (-p \mathbf{I} + \lambda_s \text{Tr}(\mathbf{E}) \mathbf{I} + 2\mu_s \mathbf{E}) = 0 \quad (19)$$

The continuity equation of the mixture phase is rewritten as

$$\nabla \cdot \left\{ \left(\frac{(\phi^w)^2}{f_{ws}} \right) \left[\nabla p - RT(\Phi - 1) \nabla \sum_{k=1}^N c^k + F_c \nabla \psi \sum_{k=1}^N z^k c^k \right] \right\} = 0 \quad (20)$$

The continuity equations of diffusive ionic concentrations are given as

$$\nabla \cdot (D_k \nabla c^k) + \left(\frac{F_c}{RT} \right) z^k \nabla \cdot (c^k D_k \nabla \psi) = 0 \quad (k = 1, 2, \dots, N) \quad (21)$$

The Poisson equation for electric potential keeps as

$$\nabla^2 \psi = - \frac{F}{\varepsilon \varepsilon_0} \sum_{k=1}^N (z^k c^k + z^f c^f) \quad (22)$$

For the present computational domain including both the hydrogels and the surrounding solution, the boundary conditions consist of the Dirichlet boundary conditions at the edges of bathing solution as

$$\psi|_{\text{Anode}} = +0.5 \text{ Ve}, \quad \text{and} \quad \psi|_{\text{Cathode}} = -0.5 \text{ Ve} \quad (23)$$

$$c^k|_{\text{Anode}} = c^k|_{\text{Cathode}} = \bar{c}_k^* \quad (24)$$

and the interfacial conditions at hydrogel–solution interfaces as

$$p|_{\text{interface}} = RT \sum_{k=1}^N (c_{\text{in-interface}}^k - c_{\text{out-interface}}^k) - p_0 \quad (25)$$

$$p|_{\text{interface}} \mathbf{I} = \lambda_s \text{Tr}(\mathbf{E}|_{\text{interface}}) \mathbf{I} + 2\mu_s \mathbf{E}|_{\text{interface}} \quad (26)$$

where \bar{c}_k^* ($k = 1, 2, \dots, N$) are the bathing solution concentrations at the anode and cathode of the externally applied electric field, $c_{\text{in-interface}}^k$ the k th ionic concentration within the hydrogels near the interfaces and $c_{\text{out-interface}}^k$ is the

k th ionic concentrations of the bathing solution near the interfaces, p_0 represents the osmotic pressure at reference configuration. It is noted that $c^f = 0$ in the exterior solution domain. The present interfacial conditions are based on the assumptions that, at the hydrogel–solution interface, the chemical potentials of hydrogels are equal to those of the bathing solution, and the mixture-phase stress is equal to zero.

For numerical examination of the presently developed MECe model with chemo-electro-mechanical coupling effects, several one-dimensional equilibrium simulations are carried out for the steady-state deformation in the thickness h direction of strip-like electric-sensitive hydrogels, when they are immersed into the bathing solution under an electric field. In the simulations it is assumed that the diffusive coefficients $D_k = D$ ($k = 1, 2, \dots, N$) and the strain here is isotropic, i.e.

$$\text{Tr}(\mathbf{E}) = 3e_{11} = 3 \frac{\partial u}{\partial x} \quad (27)$$

where e_{11} is the strain in thickness direction. Furthermore, for demonstration of the one-dimensional equilibrium deformation, an average curvature K_a , resulting from the pressure difference between the two ends of the thickness h , is defined geometrically at the middle point of the thickness (Zhou et al., 2002)

$$K_a = \frac{2(e_1 - e_2)}{h(2 + e_1 + e_2)} \quad (28)$$

where e_1 and e_2 indicate the swelling strains at the two ends of hydrogel thickness.

In the present numerical algorithms, a two-level hierarchical iteration technique is employed to solve the MECe coupled nonlinear partial differential governing equations. The inner iterations are to simultaneously compute the diffusive ion concentrations and electric potential. Then the computed results are substituted into the subsequent outer iteration loop for computation of the displacement and pressure. The fixed-charge concentration and water volume fraction can also be computed iteratively. For implementation of the two-level hierarchical iteration, a meshless approach called the Hermite–Cloud method (Li et al., 2003) is used and the remeshing technique is required due to the movement of hydrogel–solution interfaces.

3. Hermite–Cloud method (HCM)

In this section, a recently developed meshless approach—Hermite–Cloud method (Li et al., 2003) is introduced to solve the above nonlinear partial differential boundary value (PDBV) problems. As an extension of the classical reproducing kernel particle method (RKPM) (Liu et al., 1995, 1996), this meshless approach uses the Hermite theorem for construction of the interpolation functions and the point collocation technique for discretization of the PDBV problems.

For any unknown real function $f(x,y)$, such as the present k th ionic concentration c^k , electric potential ψ , fluid pressure p and solid-phase displacement u , the approximation $f(x,y)$ can be constructed by the meshless HCM

$$\begin{aligned} \tilde{f}(x, y) = & \sum_{n=1}^{N_T} N_n(x, y) f_n + \sum_{m=1}^{N_S} \left(x - \sum_{n=1}^{N_T} N_n(x, y) x_n \right) \\ & \times M_m(x, y) G x_m + \sum_{m=1}^{N_S} \left(y - \sum_{n=1}^{N_T} N_n(x, y) y_n \right) \\ & \times M_m(x, y) G y_m \end{aligned} \quad (29)$$

where N_T and $N_S (\leq N_T)$ are total numbers of discrete points covering the computational domain, and $N_n(x,y)$ are the shape functions defined as

$$\begin{aligned} N_n(x, y) = & \mathbf{B}(p_n, q_n) \mathbf{A}^{-1}(x_k, y_k) \mathbf{B}^T(x, y) \\ & \times K(x_k - p_n, y_k - q_n) \Delta S_n \quad (n = 1, 2, \dots, N_T) \end{aligned} \quad (30)$$

in which $K(x_k - p_n, y_k - q_n)$ is the kernel function defined as

$$K(x_k - p, y_k - q) = \frac{1}{\Delta x \Delta y} W^* \left(\frac{x_k - p}{\Delta x} \right) W^* \left(\frac{y_k - q}{\Delta y} \right) \quad (31)$$

$\mathbf{B}(p,q)$ is the linearly independent basis. For example for one- or two-dimensional quadratic PDBV problem, it is given, respectively, as

$$\mathbf{B}(p) = \{b_1(p), b_2(p), \dots, b_\beta(p)\} = \{1, p, p^2\} \quad (\beta = 3) \quad (32)$$

$$\begin{aligned} \mathbf{B}(p, q) = & \{b_1(p, q), b_2(p, q), \dots, b_\beta(p, q)\} \\ = & \{1, p, q, p^2, pq, q^2\} \quad (\beta = 6) \end{aligned} \quad (33)$$

and $\mathbf{A}(x_k, y_k)$ is a symmetric matrix associated with the fixed kernel centered point (x_k, y_k) and is expressed as

$$\begin{aligned} A_{ij}(x_k, y_k) = & \sum_{n=1}^{N_T} b_i(p_n, q_n) K(x_k - p_n, y_k - q_n) b_j(p_n, q_n) \\ & \times \Delta S_n \quad (i, j = 1, 2, \dots, \beta) \end{aligned} \quad (34)$$

In Eq. (31), $W^*(z)$ is called the window function and defined as a cubic spline function

$$W^*(z) = \begin{cases} 0 & 2 < |z| \\ \frac{(2 - |z|)^3}{6} & 1 \leq |z| \leq 2 \\ \left(\frac{2}{3}\right) - z^2(1 - 0.5|z|) & 0 \leq |z| \leq 1 \end{cases} \quad (35)$$

where $z = (x_k - p)/\Delta x$ or $z = (y_k - q)/\Delta y$ for the x - or y -component, Δx and Δy denote the cloud sizes of the fixed kernel centered at the point (x_k, y_k) in the x - and y -direction, respectively.

In the approximate solution (29), assuming $Gx(x, y) = \partial f(x, y) / \partial x$ and $Gy(x, y) = \partial f(x, y) / \partial y$, the discrete approximations of $Gx(x, y)$ and $Gy(x, y)$ may be given by (Li et al., 2003)

$$\begin{aligned} \tilde{G}x(x, y) &= \sum_{m=1}^{N_s} M_m(x, y) Gx_m \quad \tilde{G}y(x, y) \\ &= \sum_{m=1}^{N_s} M_m(x, y) Gy_m \end{aligned} \quad (36)$$

It is noted that, compared with the shape functions $N_n(x, y)$ constructed on β -order basis in Eq. (30), the present shape functions $M_m(x, y)$ are constructed on $(\beta - 1)$ -order basis.

The auxiliary conditions are required for the additional unknown functions $Gx(x, y)$ and $Gy(x, y)$. By imposing the first-order partial differentials with respect to the variables x and y on the approximation $f(x, y)$ expressed by Eq. (29), and using Eq. (36), we have the auxiliary conditions as

$$\begin{aligned} \sum_{n=1}^{N_T} N_{n,x}(x, y) f_n - \sum_{m=1}^{N_s} \left(\sum_{n=1}^{N_T} (N_{n,x}(x, y) x_n) \right) M_m(x, y) Gx_m \\ - \sum_{m=1}^{N_s} \left(\sum_{n=1}^{N_T} (N_{n,x}(x, y) y_n) \right) M_m(x, y) Gy_m = 0 \end{aligned} \quad (37)$$

$$\begin{aligned} \sum_{n=1}^{N_T} N_{n,y}(x, y) f_n - \sum_{m=1}^{N_s} \left(\sum_{n=1}^{N_T} (N_{n,y}(x, y) y_n) \right) M_m(x, y) Gy_m \\ - \sum_{m=1}^{N_s} \left(\sum_{n=1}^{N_T} (N_{n,y}(x, y) x_n) \right) M_m(x, y) Gx_m = 0 \end{aligned} \quad (38)$$

$$f(x, y) = Q(x, y) \quad \text{in } \Gamma_D \quad (\text{Dirichlet boundary conditions}) \quad (40)$$

$$f_n = R(x, y) \quad \text{in } \Gamma_N \quad (\text{Neumann boundary conditions}) \quad (41)$$

where L is differential operator, $f(x, y)$ unknown real function and Ω the interior domain. By the point collocation technique, the PDBV problem is discretized as

$$L\tilde{f}(x_i, y_i) = P(x_i, y_i) \quad i = 1, 2, \dots, N_\Omega \quad (42)$$

$$\tilde{f}(x_i, y_i) = Q(x_i, y_i) \quad i = 1, 2, \dots, N_D \quad (43)$$

$$\tilde{f}_n = R(x_i, y_i) \quad i = 1, 2, \dots, N_N \quad (44)$$

where N_Ω , N_D and N_N are the numbers of scattered points in the interior computational domain, and along the Dirichlet and Neumann boundaries, respectively. Thus, the total number of scattered points $N_T = (N_\Omega + N_D + N_N)$.

After substituting the approximate solutions (29) and (36) into Eqs. (42)–(44), a set of algebraic equations is obtained as follows

$$[H_{ij}]_{(N_T+2N_s) \times (N_T+2N_s)} \{F_i\}_{(N_T+2N_s) \times 1} = \{d_i\}_{(N_T+2N_s) \times 1} \quad (45)$$

where $\{d_i\}$ and $\{F_i\}$ are $(N_T + 2N_s)$ -order column vectors

$$\{F_i\}_{(N_T+2N_s) \times 1} = \{\{f_i\}_{1 \times N_T}, \{Gx_i\}_{1 \times N_s}, \{Gy_i\}_{1 \times N_s}\}^T \quad (46)$$

$$\begin{aligned} \{d_i\}_{(N_T+2N_s) \times 1} = \{\{P(x_i, y_i)\}_{1 \times N_\Omega}, \{Q(x_i, y_i)\}_{1 \times N_D}, \\ \times \{R(x_i, y_i)\}_{1 \times N_N}, \{0\}_{1 \times 2N_s}\}^T \end{aligned} \quad (47)$$

and $[H_{ij}]$ is a $(N_T + 2N_s) \times (N_T + 2N_s)$ coefficient matrix

$$[H_{ij}] = \begin{bmatrix} [LN_j(x_i, y_i)]_{N_\Omega \times N_T} & [L((x_i - \sum_{n=1}^{N_T} N_n(x_i, y_i) x_n) \mathbf{M}_j(x_i, y_i))]_{N_\Omega \times N_s} & [L((y_i - \sum_{n=1}^{N_T} N_n(x_i, y_i) y_n) \mathbf{M}_j(x_i, y_i))]_{N_\Omega \times N_s} \\ [N_j(x_i, y_i)]_{N_D \times N_T} & [0]_{N_D \times N_s} & [0]_{N_D \times N_s} \\ [0]_{N_N \times N_T} & [\mathbf{M}_j(x_i, y_i)]_{N_N \times N_s} \mathbf{i}_x & [\mathbf{M}_j(x_i, y_i)]_{N_N \times N_s} \mathbf{i}_y \\ [N_{j,x}(x_i, y_i)]_{N_s \times N_T} & [-\sum_{n=1}^{N_T} N_{n,x}(x_i, y_i) x_n \mathbf{M}_j(x_i, y_i)]_{N_s \times N_s} & [-\sum_{n=1}^{N_T} N_{n,x}(x_i, y_i) y_n \mathbf{M}_j(x_i, y_i)]_{N_s \times N_s} \\ [N_{j,y}(x_i, y_i)]_{N_s \times N_T} & [-\sum_{n=1}^{N_T} N_{n,y}(x_i, y_i) x_n \mathbf{M}_j(x_i, y_i)]_{N_s \times N_s} & [-\sum_{n=1}^{N_T} N_{n,y}(x_i, y_i) y_n \mathbf{M}_j(x_i, y_i)]_{N_s \times N_s} \end{bmatrix} \quad (48)$$

So far the formulation of the meshless Hermite–Cloud method has been completed. By the point collocation technique to discretize the PDBV problems, it employs the Hermite interpolation theorem to construct the approximate unknown function $f(x, y)$ by Eq. (29), and couples the first-order differential functions $Gx(x, y)$ and $Gy(x, y)$ expressed by Eq. (36) and the auxiliary conditions (37) and (38).

In general, the PDBV problems in engineering may be written as

$$L f(x, y) = P(x, y) \quad \text{in } \Omega \quad (39)$$

where \mathbf{i}_x and \mathbf{i}_y are outward normal vectors. The complete set of the above algebraic equations can be solved numerically to obtain $(N_T + 2N_s)$ point values $\{F_i\}$. Accordingly, the approximate solutions $f(x, y)$ and the corresponding first-order differentials $Gx(x, y)$ and $Gy(x, y)$ can be computed through Eqs. (29) and (36).

4. Numerical results and discussions

To investigate the swelling equilibrium behavior of electric-stimulus responsive hydrogels by the multiphysic

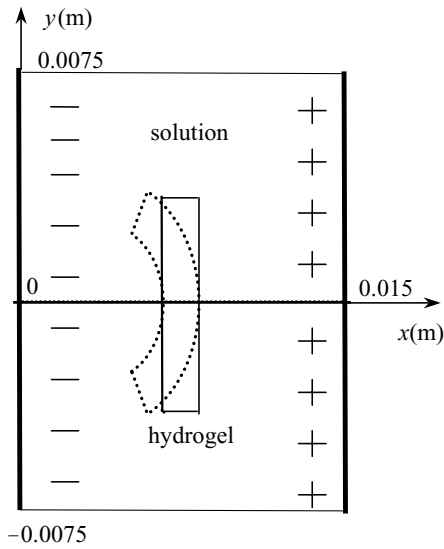


Fig. 2. Bending deformation of hydrogel strip in bathing solution subject to externally applied electric field.

MECe model, one-dimensional steady-state numerical simulations are carried out along the x -axis for a hydrogel strip immersed into the NaCl solution subject to an externally applied electric field, as shown in Fig. 2. In the solution domain $x(m) \in [0, 0.005] \cup [0.010, 0.015]$, the Dirichlet boundary conditions of the solution ion concentrations and electrical potential at anode and cathode are imposed at $x = 0$ and 15×10^{-3} m and expressed by the Eqs. (23) and (24). The specified parameters are $\phi_0^w = 0.8$, $\epsilon_0 = 8.854 \times 10^{-12} \text{ C}^2/(\text{N m}^2)$, $\epsilon = 80$, $(3\lambda + 2\mu) = 1.2 \times 10^5 \text{ Pa}$, $\Phi = 1$, $\gamma_k = 1$ ($k = 1, 2, \dots, N$), $T = 293 \text{ K}$, $R = 8.314 \text{ J}/(\text{mol K})$ and $F_c = 9.6487 \times 10^4 \text{ C}/\text{mol}$.

When the fixed-charge concentration $c_0^f = 10 \text{ mM}$ with the valance $z^f = -1$, the thickness of the hydrogel strip $h = 5 \times 10^{-3} \text{ m}$, and the ionic concentrations of the bathing

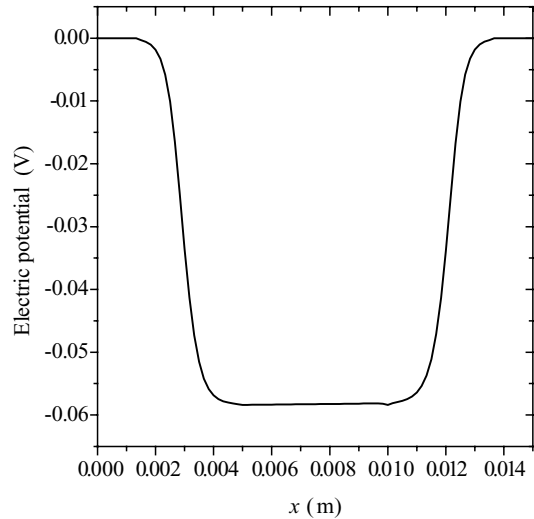


Fig. 4. Distribution of electric potential without external electric field.

solution $\bar{c}_{\text{Na}^+}^* = \bar{c}_{\text{Cl}^-}^* = 1 \text{ mM}$, the simulated results are obtained and shown in Figs. 3 and 4 for the distributions of the diffusive ionic concentrations and electrical potential, where no external electric field is applied ($V_e = 0$). It is observed from the figures that the electroneutrality exists in the bathing solution and the hydrogel strip with fixed charge groups. It is also known that the uniform distributions of ionic concentrations and electric potential within hydrogels result in the uniform swelling (no bending) deformation of hydrogel strip.

When the external electric field $V_e = 0.2 \text{ V}$ with $\psi = +0.1 \text{ V}$ at anode and $\psi = -0.1 \text{ V}$ at cathode is applied as shown in Fig. 2, $c_0^f = 10 \text{ mM}$, $z^f = -1$, $h = 5 \times 10^{-3} \text{ m}$, $\bar{c}_k^* = 1 \text{ mM}$, and no effect of mechanical deformation is considered, the variations of diffusive ionic concentrations and electrical potential are numerically simulated and depicted in Figs. 5 and 6. The present hydrogel is charged by fixing

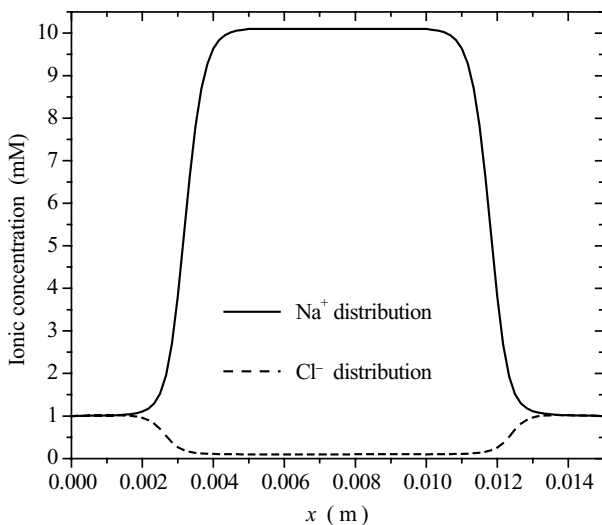


Fig. 3. Distribution of ionic concentrations without external electric field.

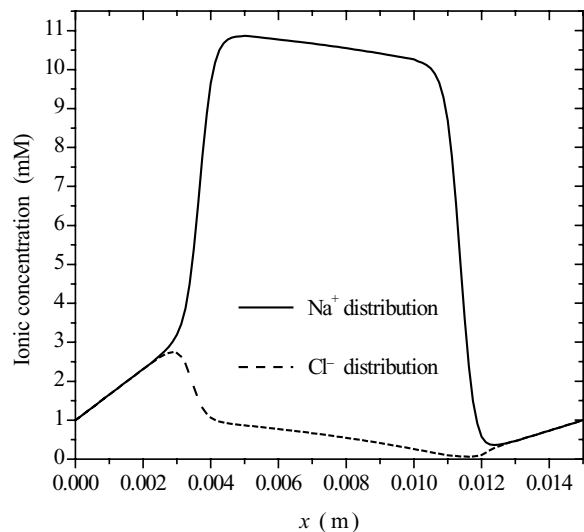


Fig. 5. Distribution of ionic concentrations with external electric field.

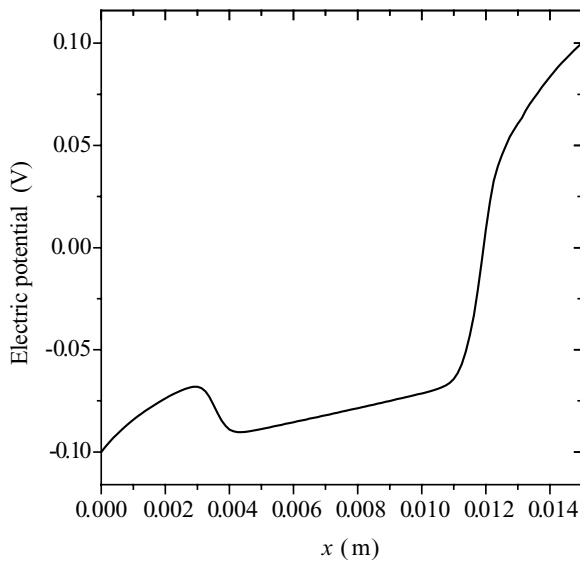


Fig. 6. Distribution of electric potential with external electric field.

the anions ($z^f = -1$) on the polymer chains of the hydrogel. The cations thus, are the dominant mobile ions within the hydrogel. When the external electric field is applied, the cations transport from anode side to cathode side until the equilibrium state attains. Therefore, the cation concentration increases near the hydrogel edge close to the cathode and decreases near the hydrogel edge close to the anode. Since the electric current is constant in the equilibrium state (Doi et al., 1992), this requires the electro-neutrality. As a result, the anion concentration also increases near the cathode side and decreases near the anode side. In other words, with increasing the distance from the cathode, the diffusive ionic concentration within the hydrogels decreases. With increasing the distance from the anode, the diffusive ionic concentration in the hydrogel strip increases. Fig. 5 depicts well the above phenomena. It is also seen from Fig. 5 that the interface ion concentration difference between the interior hydrogel and exterior bathing solution near the anode is larger than that near the cathode. Additionally, it is observed from Figs. 5 and 6 that, corresponding to the larger number of mobile ions, the hydrogel has the higher conductivity than the solution. The increase of the electric potential in the hydrogel is smaller than that in the solution. The smaller change of the electric potential in the hydrogel is compensated by a smaller step at the cathode side and a larger one at the anode side of the hydrogel, as shown in Fig. 6. Namely the Donnan potential $\Delta\psi$ has a more negative value at anode side and a less negative value at the cathode side, compared with the initial value without applied electric field. As such, the larger difference of electric potential on the anode side leads to the larger interface concentration difference near the anode side. Furthermore, compared with the concentration difference on the cathode side, the larger concentration difference results in the larger osmotic pressure on the anode side. The difference of osmotic pressure between the anode and cathode sides makes the hydrogel have a bending deformation. These

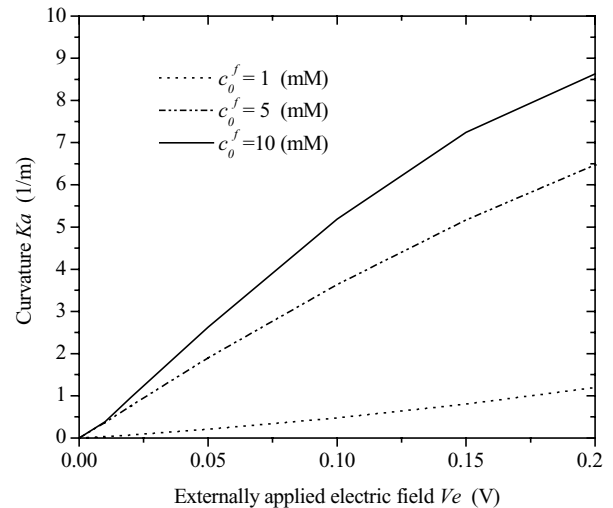


Fig. 7. Effect of fixed charge on the variation of average curvature K_a against externally applied electric field.

simulated results are validated by the experiment (Homma et al., 2001; Wallmersperger and Kroeplin, 2001). Therefore, it is concluded that the presently simulated electric-potential distribution agrees well with Wallmersperger's FEM simulations and is also acceptable when compared with the experimental data (Wallmersperger and Kroeplin, 2001).

Fig. 7 is achieved to study the mechanical deformation of the hydrogel strip with $h = 5 \times 10^{-3}$ m. For $\bar{c}_k^* = 1$ mM, the figure illustrates the variation of the average curvature K_a against the externally applied electric field Ve for different fixed-charge concentrations $c_0^f = 1, 5$ and 10 mM with $z^f = -1$. It is seen that, with the increase of the externally applied electric voltage, the differences of concentrations and electric potential increase between the hydrogel strip and the bathing solution. As such, the average curvature K_a increases almost linearly and the bending deformation becomes larger, which are in good agreement with the experimental phenomena (Homma et al., 2000; Sun and Mak, 2001; Fei et al., 2002).

Fig. 8 demonstrates the influence of the externally applied electric field Ve on the relation between the average curvature K_a and the fixed-charge concentration c_0^f , where $z^f = -1$, $h = 5 \times 10^{-3}$ m, $\bar{c}_k^* = 1$ mM, $Ve = 0.02, 0.1$ and 0.2 V, namely $\psi = +0.01, +0.05$ and $+0.1$ V at anode, $\psi = -0.01, -0.05$ and -0.1 V at cathode, respectively. It is known that, for a given applied voltage Ve , the average curvature K_a increases with the fixed-charge concentration c_0^f . The computed results are examined by the experiment (Homma et al., 2000). Furthermore, in order to ascertain the influence of the externally applied electric field Ve on the relation between the average curvature K_a and bathing-solution concentration \bar{c}_k^* , Fig. 9 is plotted when $c_0^f = 10$ mM, $z^f = -1$, $h = 5 \times 10^{-3}$ m and $Ve = 0.02, 0.10$ and 0.20 V, respectively. An optimal \bar{c}_k^* value is observed when the hydrogel strip reaches the largest bending deformation. If the concentration \bar{c}_k^* of the bathing solution is larger than the computed

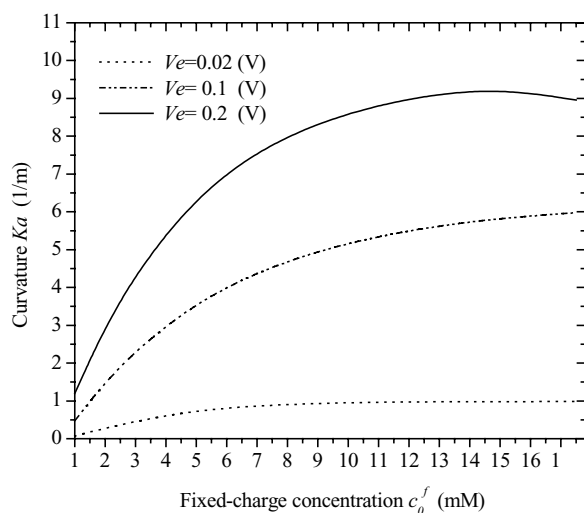


Fig. 8. Effect of externally applied electric field on the variation of average curvature K_a against fixed charge concentration.

optimal concentration, the bending deformation of hydrogel strip decreases with increasing \bar{c}_k^* . The present simulations agree well with the experimental results (Homma et al., 2000, 2001; Sun and Mak, 2001; Fei et al., 2002).

For $c_0^f = 10$ mM, $z^f = -1$, and $\bar{c}_k^* = 1$ mM, Fig. 10 shows the relation between the average curvature K_a and the thickness h of hydrogel strip for various externally applied electric field, $V_e = 0.02, 0.1$ and 0.2 V, respectively. It is presented that the average curvature K_a of the hydrogel strip decreases rapidly with increasing thickness h , which is in consistence with the experiment (Homma et al., 2000, 2001).

In order to investigate the effect of multivalent electrolyte on the average curvature K_a of bending deformation, the hydrogel strip is immersed into the bathing solutions of CuSO_4 and Na_2SO_4 , respectively. For $V_e = 0.2$ V, $c_0^f = 10$ mM, $z^f = -1$ and $h = 5 \times 10^{-3}$ m, Fig. 11 is depicted. It is seen

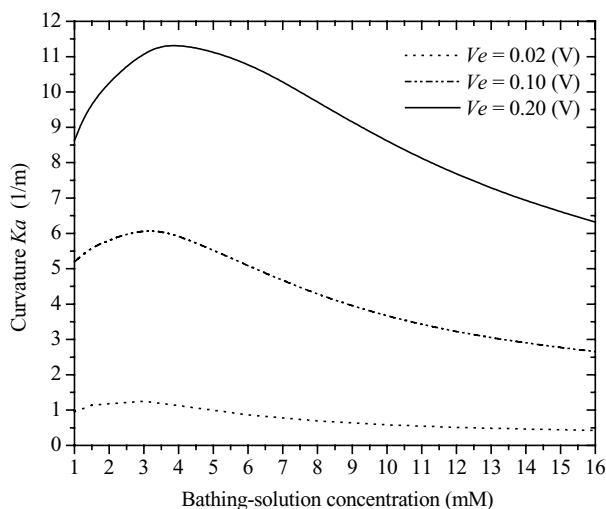


Fig. 9. Effect of externally applied electric field on the variation of average curvature K_a against bathing-solution concentration.

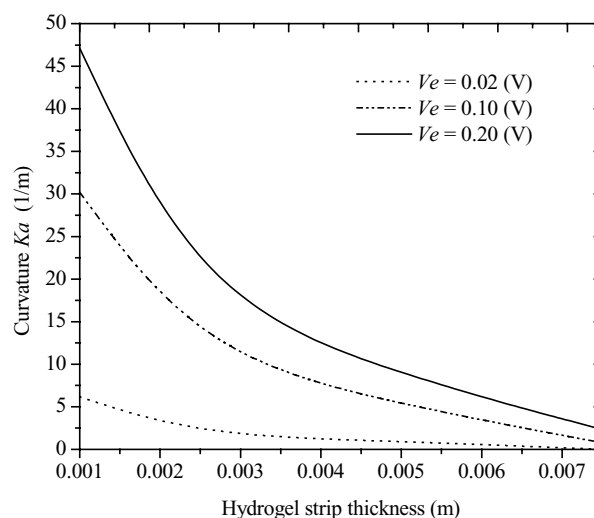


Fig. 10. Effect of externally applied electric field on the variation of average curvature K_a against the thickness of hydrogel strip.

clearly that the average curvature K_a of the hydrogel strip in Na_2SO_4 solution is larger than that in CuSO_4 , which is also in agreement with the experimental results (Homma et al., 2000, 2001). When the hydrogel strip is placed into the electrolyte solution with an applied electric field, the decrease of the univalent cation Na^+ concentration within the hydrogel strip at the anode is much larger than that of the bivalent cation Cu^{2+} concentration subject to the same electric field. The more the counterion decreases, the larger bending deformation the hydrogel yields. Therefore, it is reasonable that the average curvature K_a for univalent electrolyte solution Na_2SO_4 is larger than that for bivalent electrolyte solution CuSO_4 .

For examination of the presently developed MECe model, as shown in Fig. 12, the simulated results are compared numerically with experimental data (Zhou et al., 2002) for

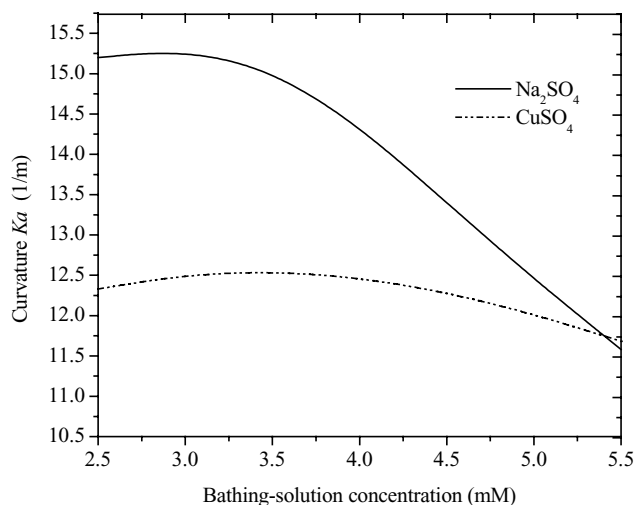


Fig. 11. Effect of multivalent electrolyte on the variation of average curvature K_a against bathing-solution concentration.

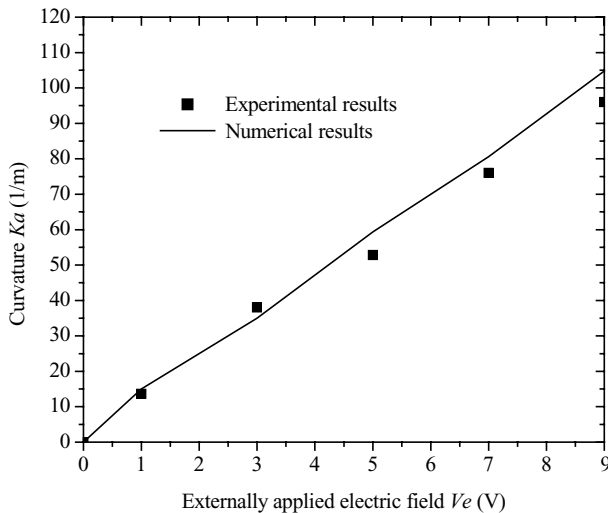


Fig. 12. Comparison of simulated results with experimental data (Zhou et al., 2002) for the hydrogel strip with positive fixed charge group.

the positive fixed charge groups ($z^f = +1$) attached on the polymer network of the hydrogel strip. The parameters used are $\phi_0^w = 0.8$, $\varepsilon_0 = 8.854 \times 10^{-12} \text{ C}^2/(\text{Nm}^2)$, $\varepsilon = 80$, $(3\lambda + 2\mu) = 1.2 \times 10^5 \text{ Pa}$, $h = 1.0 \times 10^{-3} \text{ m}$, $c_0^f = 20 \text{ mM}$, $\bar{c}_k^* = 5.5 \text{ mM}$, $\Phi = 1$, $\gamma_k = 1$ ($k = 1, 2, \dots, N$), $T = 278 \text{ K}$, $R = 8.314 \text{ J}/(\text{mol K})$. The distance between two electrodes is $2.0 \times 10^{-2} \text{ m}$ and only univalent ions are considered. As depicted in Fig. 12, the average curvatures K_a of both the computed and experimental results increase linearly with the externally applied electric field V_e . Both the results meet well under 5 V applied electric field. However, they seem to have different trends above 5 V. As well known, the bending deformation of the present electric-sensitive hydrogels depends directly on many parameters, including the voltage of applied electric field, electrolyte composition, fixed charge, chemical reactions, temperature, heat conduction, ionic diffusion and convection. As a preliminary work with isotropy assumption, the influences of chemical reactions, heat conduction and temperature have not been included in the presently developed mathematical MECe model. This simplification is feasible under low voltage (such as 5 V) of the applied electric field. However, with the increase of the applied electric voltage, these nonlinear effects become more and more significant (Snita et al., 2001) and they should, thus be considered. Probably, these are the main reasons for the different trends above 5 V between the experimental data and the numerical results. Anyway, the present comparisons achieve very good agreements between the simulated results and experimental data (Zhou et al., 2002).

5. Conclusion

In this paper, a multiphysics mathematical model, termed the MECe model, has been developed with considera-

tion of chemo-electro-mechanical coupling effects for the simulation of the responsive behavior of electric-sensitive hydrogels when they are immersed into a bathing solution subject to an externally applied electric field. The formulation is able to describe the swelling and shrinking as well as bending deformation of the hydrogel, the distributions of diffusive ion concentrations and electric potential in both the interior hydrogel and the exterior solution. One-dimensional numerical simulations are carried out for a hydrogel strip and the influences of physical parameters on the deformed hydrogel strip are also discussed. The numerically simulated results demonstrate good agreements with experimental data and published FEM solutions. They validate the presently developed MECe models.

References

- Baldi, A., Gu, Y., Loftness, P.E., et al., 2002. A hydrogel-actuated smart micro-valve with a porous diffusion barrier back-plate for active flow control. *Proc. MEMS* 2002, 105–108.
- Beebe, D.J., Moore, J., Bauer, J.M., et al., 2000. Functional structures for autonomous flow control inside micro-fluidic channels. *Nature* 404, 588–590.
- Brock, D., Lee, W., Segalman, D., Witkowski, W., 1994. A dynamic model of a linear actuators based on polymer hydrogel. *J. Intell. Mater. Syst. Struct.* 5, 764–771.
- de Gennes, P.G., Okumura, Ko, Shahinpoor, M., Kim, K.J., 2000. Mechanoelectric effects in ionic gels. *Europhys. Lett.* 50 (4), 513–518.
- Doi, M., Matsumoto, M., Hirose, Y., 1992. Deformation of ionic polymer gels by electric fields. *Macromolecules* 25, 5504–5511.
- Eichenbaum, G.M., Kiser, P.M., Simon, S.A., Needham, D., 1998. pH and ion-triggered volume response of anionic hydrogel microspheres. *Macromolecules* 31, 5084–5093.
- Fei, J.Q., Zhang, Z.P., Gu, L.X., 2002. Bending behavior of electroresponsive poly(vinyl alcohol)/poly(acrylic acid) semi-interpenetrating network hydrogel fibers under an electric stimulus. *Polym. Int.* 51, 502–509.
- Grimshaw, P.E., Nussbaum, J.H., Grodzinsky, A.J., et al., 1990. Kinetics of electrically and chemically induced swelling in polyelectrolyte gels. *J. Chem. Phys.* 93, 4462–4472.
- Gu, W.Y., Lai, W.M., Mow, V.C., 1998. A mixture theory for charged-hydrated soft tissues containing multi-electrolytes: passive transport and swelling behaviors. *J. Biomech. Eng.* 120, 169–181.
- Gu, W.Y., Lai, W.M., Mow, V.C., 1999. Transport of multi-electrolytes in charged hydrated biological soft tissues. *Transport Porous Media* 34, 143–157.
- Homma, M., Seida, Y., Nakano, Y., 2000. Evaluation of optimum condition for designing high performance electro-driven polymer hydrogel systems. *J. Appl. Polym. Sci.* 75, 111–118.
- Homma, M., Seida, Y., Nakano, Y., 2001. Effect of ions on the dynamic behavior of an electrodriven ionic polymer hydrogel membrane. *J. Appl. Polym. Sci.* 82, 76–80.
- Hon, Y.C., Lu, M.W., Xue, W.M., Zhou, X., 1999. A new formulation and computation of the triphasic model for mechano-electrochemical mixtures. *Comput. Mech.* 24 (3), 155–165.
- Kim, S.Y., Shin, H.S., 1999. Properties of electroresponsive poly(vinyl alcohol)/poly(acrylic acid) IPN hydrogels under an electric stimulus. *J. Appl. Polym. Sci.* 73, 1675–1683.
- Kim, B., Peppas, N.A., 2002. Synthesis and characterization of pH-sensitive glycopolymers for oral drug delivery systems. *J. Biomater. Sci. Polym. Edn.* 13 (11), 1271–1281.

- Lai, W.M., Hou, J.S., Mow, V.C., 1991. A triphasic theory for the swelling and deformation behaviors of articular cartilage. *J. Biomech. Eng.* 113, 245–258.
- Lai, W.M., Mow, V.C., Sun, D.D., Ateshian, G.A., 2000. On the electric potentials inside a charged soft hydrated biological tissues: streaming potential versus diffusion potential. *J. Biomech. Eng.* 122, 336–346.
- Li, H., Ng, T.Y., Cheng, J.Q., Lam, K.Y., 2003. Hermite–Cloud: a novel true meshless method. *Comput. Mech.* 32, 339–350.
- Liu, W.K., Chen, Y., Chang, C.T., Belytschko, T., 1996. Advances in multiple scale kernel particle methods. *Comput. Mech.* 18, 73–111.
- Liu, W.K., Jun, S., Li, S., Adde, J., Belytschko, T., 1995. Reproducing kernel particle methods for structural dynamics. *Int. J. Numerical Methods Eng.* 38, 1665–1679.
- Liu, W.K., Jun, S., Zhang, Y.F., 1995. Reproducing kernel particle methods. *Int. J. Numerical Methods Eng.* 20, 1081–1106.
- Miyata, T., Asami, N., Uragami, T., 1999. A reversible antigen-responsive hydrogel. *Nature* 399, 766–769.
- Mow, V.C., Ateshian, G.A., Lai, W.M., Gu, W.Y., 1998. Effects of fixed charges on the stress-relaxation behaviors of hydrated soft tissues in a confined compression problem. *Int. J. Solids Struct.* 35, 4945–4962.
- Nemat-Nasser, S., Li, J.Y., 2000. Electromechanical response of ionic polymer–metal composites. *J. Appl. Phys.* 87 (7), 3321–3331.
- Shahinpoor, M., 1994. Continuum electromechanics of ionic polymer gels as artificial muscles for robotic applications. *Smart Mater. Struct.* 3, 367–372.
- Shahinpoor, M., 1995. Micro-electro-mechanics of ionic polymer gels as electrically controlled artificially muscles. *J. Intell. Mater. Syst. Struct.* 6, 307–314.
- Shahinpoor M., 2000. Electro-mechanics of ionic-elastic beams as electrically controllable artificial muscles. In: *Symposium on Electroactive Polymer Actuators and Devices—Proceedings of the SPIE*, vol. 3987, pp. 109–121.
- Shiga, T., Hirose, Y., Okada, A., Kurauchi, T., 1993. Bending of ionic polymer gel caused by swelling under sinusoidally varying electric fields. *J. Appl. Polym. Sci.* 47, 113–119.
- Snita, D., Paces, M., Lindner, J., Kosek, J., Marek, M., 2001. Nonlinear behaviour of simple ionic systems in hydrogel in an electric field. *Faraday Discuss.* 120, 53–66.
- Sun, D.N., Gu, W.Y., Guo, X.E., et al., 1999. A mixed finite element formulation of triphasic mechano-electrochemical theory for charged hydrated biological soft tissues. *Int. J. Numerical Methods Eng.* 45, 1375–1402.
- Sun, S., Mak, A.F.T., 2001. The dynamical response of a hydrogel fiber to electrochemical stimulation. *J. Polym. Sci. Part B: Polym. Phys.* 39, 236–246.
- Wallmersperger, T., Kroeplin, B., 2001. Modeling and analysis of the chemistry and electromechanics. In: Bar-Cohen, Y. (Ed.), *Electroactive Polymer Actuators as Artificial Muscles*. SPIE Press, pp. 285–307.
- Wang, C., Li, Y., Hu, Z., 1997. Swelling kinetics of polymer gels. *Macromolecules* 30, 4727–4732.
- Yuan, Z., Li, H., Ng, T.Y., Chen, J., 2002. A coupled multi-field formulation for stimuli-responsive hydrogel subject to electric field. *Recent Advances in Computational Science and Engineering—Proceeding of the International Conference on Scientific & Engineering Computation (IC-SEC)*. 2002, pp. 884–887.
- Zhou, X., Hon, Y.C., Sun, S., Mak, A.F.T., 2002. Numerical simulation of the steady-state deformation of a smart hydrogel under an external electric field. *Smart Mater. Struct.* 11, 459–467.